Spin-Labeling Studies of the Conformational Changes in the Vicinity of D36, D38, T46, and E161 of Bacteriorhodopsin during the Photocycle

Thomas Rink,* Jens Riesle,# Dieter Oesterhelt,# Klaus Gerwert,* and Heinz-Jürgen Steinhoff*
*Lehrstuhl für Biophysik, Ruhr-Universität Bochum, 44780 Bochum, and #Max-Planck-Institut für Biochemie, 82152 Martinsried, Germany

ABSTRACT Electron paramagnetic resonance (EPR) spectroscopy of site-directed spin-labeled bacteriorhodopsin mutants is used to study structural changes during the photocycle. After exchange of the native amino acids D36 and D38 in the A-B loop, E161 in the E-F loop, and T46 in the putative proton channel by cysteines, these positions were modified by a methanethiosulfonate spin label. Time-resolved EPR spectroscopy reveals spectral changes during the photocycle for the mutants with spin labels attached to C36, C161, and C46. A comparison of the transient spectral amplitudes with simulated EPR difference spectra shows that the detected signals are due to changes in the spin label mobility and not to possible polarity changes in the vicinity of the attached spin label. The kinetic analysis of the EPR and the visible data with a global fitting procedure exhibits a structural rearrangement near position 161 in the E-F loop in the M state. The environmental changes at positions 36 and 46, however, occur during the M-to-N transition. All structural changes reverse with the recovery of the BR ground state. No structural changes are detected with a spin label attached to C38.

INTRODUCTION

The retinal protein bacteriorhodopsin (BR) acts as a light-driven proton pump in the cell membrane of halobacteria (for reviews see, e.g., Tittor, 1991; Lanyi, 1993). The absorption of a photon by the intrinsic chromophore all-*trans* retinal leads to its 13-*cis* isomerization, which initiates a series of proton transfer reactions inside the protein. These reactions result in a net translocation of one proton across the membrane after thermal reisomerization of the chromophore and completion of the catalytic cycle. Intermediates of the thermoreversible photochemical reaction in BR detected by optical spectroscopy were arranged in so-called photocycles. One widely accepted model of the photocycle is a linear sequence of intermediates, most of which have significant back-reactions (Varo and Lanyi, 1991; Lozier et al., 1992; Hessling et al., 1993). The different intermediates are characterized by specific configurational states of the retinal, the protonation state of the retinal and certain amino acid side chains, and the conformation of the protein. After light-induced isomerization, the molecule passes through the short-lived intermediates J, K, and L before it reaches the M state in 50 μs at room temperature. A further differentiation of the intermediates occurs in the M state and is suggested for the N state. In the M_1 and M_2 states, the retinal Schiff base is unprotonated and must be oriented alternatively toward the proton release pathway and toward the proton uptake pathway (e.g., Schulten and Tavan, 1978; Gerwert and Siebert, 1986; Oesterhelt et al., 1992; Lanyi, 1993). N_1 and N_2 are suggested to be states of N before and after proton uptake at the cytoplasmic surface (Zimanyi et al., 1993). The study of the intermediates has provided extensive information about the proton transfer steps (for a review see, e.g., Lanyi, 1993). Central events are the protonation of D85 by the Schiff base (Braiman et al., 1988; Gerwert et al., 1989), and the reprotonation of the Schiff base by D96 (Gerwert et al., 1989, 1990). However, one of the remaining questions is the nature of the protein conformational change (Kataoka et al., 1994) detected by diffraction studies (Koch et al., 1991; Nakasako et al., 1991; Subramaniam et al., 1993). The most prominent features of the structural change observed in wild-type BR are a significant rearrangement of helix G and minor changes close to helices B, C, and F. The D96N or D96G mutants show an additional significant tilt of helix F. The rise and decay of these conformational changes could not be followed; they are already present in the M state. The most prominent amide band changes detected by Fourier transform infrared (FTIR) spectroscopy in the wild-type BR reveal the largest peptide bond movements of the bacteriorhodopsin backbone occurring during the M-to-N transition (Gerwert et al., 1990; Souvignier and Gerwert, 1992; Rothschild et al., 1993). Further analysis of these structural changes is required for a better understanding of the underlying molecular events.

Site-directed spin labeling (SDSL) (Hubbell and Altenbach, 1994) offers a complementary approach to localizing and resolving structural changes with a time resolution sufficient to follow the sequence of intermediates in the second half of the photocycle. Electron paramagnetic resonance (EPR) experiments with a spin label attached to the cysteine in the cytoplasmic C-D interhelical loop of the BR mutant V101C reveal spectral changes, which occur after the formation of the M state. They are reversed with the recovery of the ground state (Steinhoff et al., 1994). However, no spectral changes were found at positions 105 in the same loop or 72 in the B-C interhelical loop at the extracellular surface of the protein. To further map the confor-

Received for publication 3 February 1997 and in final form 28 April 1997.
Address reprint requests to Dr. Heinz-Jurgen Steinhoff, Lehrstuhl für Biophysik, Ruhr-Universität Bochum, Gebaude ND/04-Nord, D-44780 Bochum, Germany. Tel.: 49-234-7004463; Fax: 49-234-7094238; E-mail: steinhbt@rz.ruhr-uni-bochum.de.

0006-3495/97/08/983/11 $2.00

mational changes and characterize their relationship to the different proton transfer steps, we report here time-resolved EPR studies with spin labels attached to positions D36C and D38C in the A-B interhelical loop, E161C in the E-F interhelical loop on the cytoplasmic surface, and T46C in the putative proton channel of BR.

MATERIALS AND METHODS

Mutagenesis, expression, and spin labeling

Site-specific mutants of bacteriorhodopsin D36C, D38C, E161C, and T46C were prepared according to the method of Ferrando et al. (1993). Mutagenesis was followed by transformation and homologous expression in *Halobacterium salinarium* strains HN5 (Rumpel and Oesterhelt, unpublished observations) and L33 (Wagner et al., 1981), with the help of the shuttle plasmid pEF 191. Mutated proteins were isolated as purple membrane sheets according to the method of Oesterhelt and Stoeckenius (1974). The mutations were confirmed from *H. salinarium* transformants by sequencing the polymerase chain reaction-amplified bop genes from isolated total DNA.

The spin label (1-oxyl-2,2,5,5-tetramethylpyrroline-3-methyl)methanethiosulfonate (MTSSL); Reanal, Budapest) was covalently attached to the cysteines of the membrane-bound BR mutants to yield the spin-label side chain R1 (Fig. 1 *a*). For this purpose, 10 μl of a solution of 100 mM MTSSL in acetonitrile was added to a 0.5-ml suspension of membranes in 0.1 M phosphate buffer, 0.1 M NaCl, pH 7.4, resulting in a spin label:BR ratio of 10:1. The samples were then incubated at room temperature for 12 h. Afterward, the noncovalently bound spin label was removed by filtration of the membrane suspension through a Sephadex G150 column. The labeled cysteine/BR ratio estimated from double integration of the EPR spectra and optical spectroscopy of BR was found to be close to 1 for all samples.

EPR and optical measurements

EPR spectra were recorded with a homemade X-band EPR spectrometer equipped with an AEG H_{103} rectangular cavity and a Bruker B-NM 12 B-field meter. The BR sample was loaded into a flat EPR quartz capillary

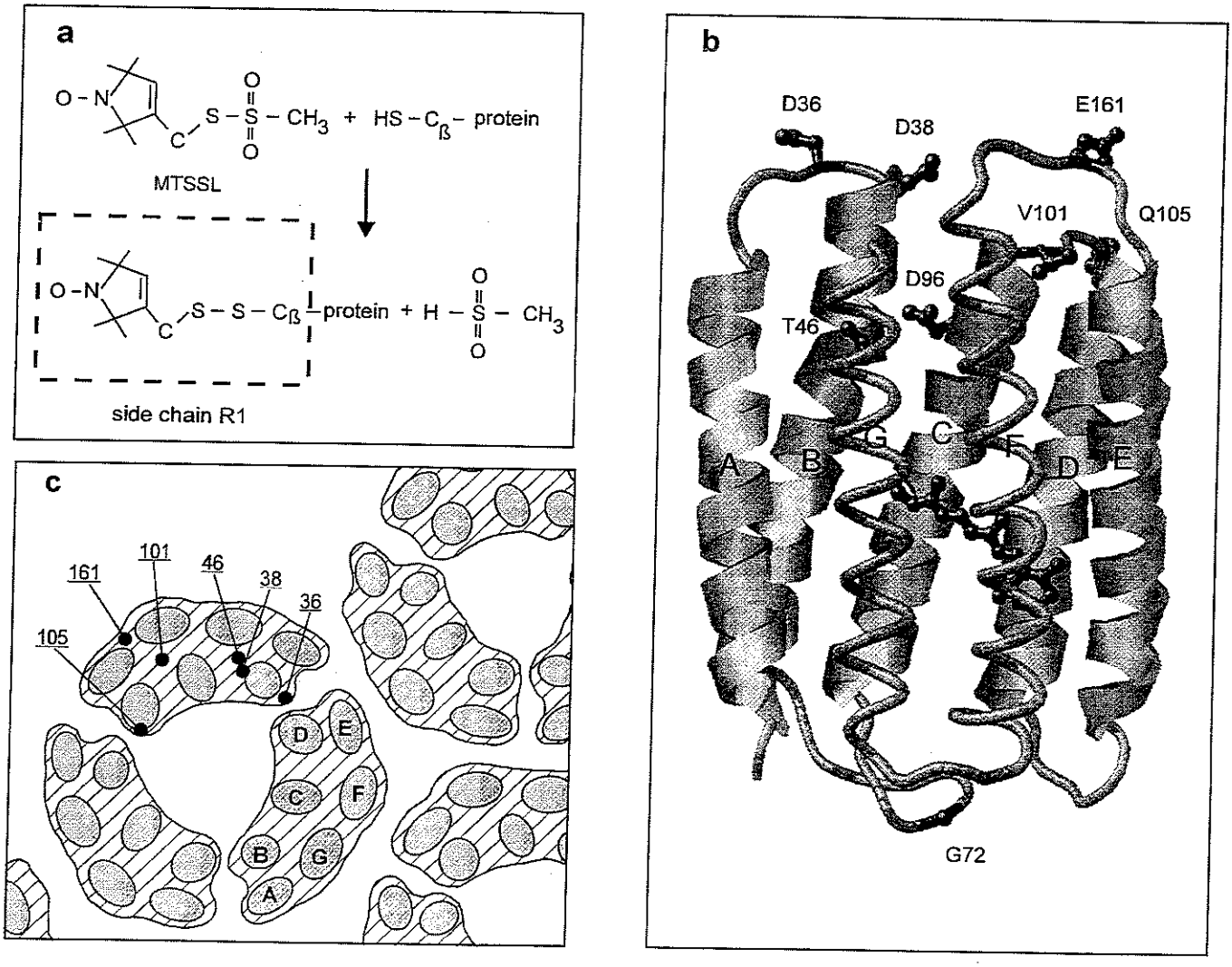

FIGURE 1 (*a*) The spin label MTSSL selectively reacts with the cysteine group of a protein to yield the modified amino acid side chain R1. (*b*) Model of the bacteriorhodopsin backbone according to the data of Grigorieff et al. (1996). Side chains of amino acids discussed in the text and the chromophore retinal are indicated. (*c*) Schematic display of the top view of the cytoplasmic structure of BR in the native purple membrane (Grigorieff et al., 1996). Each monomer within a trimer is highlighted by a surrounding line, and the positions of the transmembrane helices are shown as grey ellipses. The numbers indicate the positions of the C_β-atoms of the modified amino acids.

at a final concentration of 200–500 μM. Spectra were taken at 293 K with a modulation amplitude of 1.5 G for the continuous wave (cw) spectra, and 3 G for time-resolved experiments. After analog-to-12-bit digital conversion, the data were processed in a personal computer. Flash irradiation of the sample at 540 nm was performed through the resonator coupling hole by means of an excimer-pumped dye laser (Lambda Physik, Göttingen, Germany). Alternatively, light from a homemade flashlight (flash energy 80 J, flash duration 40 μs) was filtered through a cutoff filter (OG 435) and focused on the sample through the resonator mesh. The time constant of the phase-sensitive detector was set at 100 μs. Distortions of the EPR signal transients due to the discharge, which were visible during the first millisecond after the flash, were minimized by correction with transients recorded at magnetic field values outside the paramagnetic resonance.

EPR spectral simulation and the fitting of simulated spectra to experimental data were performed by using the EPR spectra simulation program written by Freed (1976), which was included in a homemade nonlinear, steepest-descent-fitting algorithm.

Transient absorbance changes in the visible spectrum were recorded at 11 wavelengths between 405 nm and 665 nm (405, 415, 450, 470, 488, 515, 550, 580, 605, 635, and 665 nm) with a homemade optical set-up. Depending on the signal-to-noise ratio, the transient signals determined in the visible and the EPR spectral changes were sampled between 50 and 2000 times. The bandwidth of the amplifier was reduced to a time constant of 10 μs. The repetition rate was set between 0.5 s^{-1} and 0.06 s^{-1}, depending on the photocycle duration of the respective mutant. The time courses of the transient optical absorbance changes and the transient EPR spectral changes were analyzed by a homemade global fitting procedure (Maurer et al., 1987; Souvignier and Gerwert, 1992).

RESULTS

Characterization of the spin-labeled BR mutants

A model of the BR molecule based on the data of Grigorieff et al. (1996) is shown in Fig. 1 *b*. Fig. 1 *c* displays a schematic view of the cytoplasmic top of BR in the native purple membrane. Those amino acid positions that were replaced by spin-labeled cysteines are indicated. Position D36 is located in the A-B loop, close to its center. Only two amino acids apart, D38 provides a position at the cytoplasmic end of the B helix. E 161 is located in the E-F loop, and T46 provides an amino acid position in the interior of the protein between the proton donor D 96 and the Schiff base. Opposite the position of E161, amino acid V101 is located in the C-D loop. Spin labels attached to C101 were shown to exhibit large EPR spectral changes during the photocycle (Steinhoff et al., 1994), which were interpreted as transient conformational changes in bacteriorhodospin. However, no spectral changes were detected with labels at position 105 at the cytoplasmic end of helix D or at position 72 at the extracellular side of the molecule (Steinhoff et al., 1994).

After exchange of the natural amino acids at positions 36, 38, 46, or 161 by cysteines, these positions were spin labeled with MTSSL to yield side chain R1 (cf. Fig. 1 *a*). The shape of the continuous wave (cw) EPR absorption spectrum of the spin-labeled protein reflects the nitroxide motion. At room temperature, bond rotations in the R1 side chain occur at a rate sufficient to produce motional averaging of the nitroxide magnetic parameters (Altenbach et al., 1989). Thus the reorientational motion is determined by the interaction of the nitroxide with the secondary and tertiary structure of the binding site environment and the flexibility of the binding site itself (Miick et al., 1991, 1993; Todd and Millhauser, 1991; Steinhoff and Hubbell, 1996). The spectrum of C36R1 (Fig. 2 *a*) reveals two components that are due to different mobilities of the nitroxide. The most prominent peaks of the low-field and the high-field lines reflect a very high mobility of the R1 side chain. A second component that is visible in both field regions indicates the presence of a nitroxide orientation with a higher degree of intermolecular or intramolecular interaction. Compared to

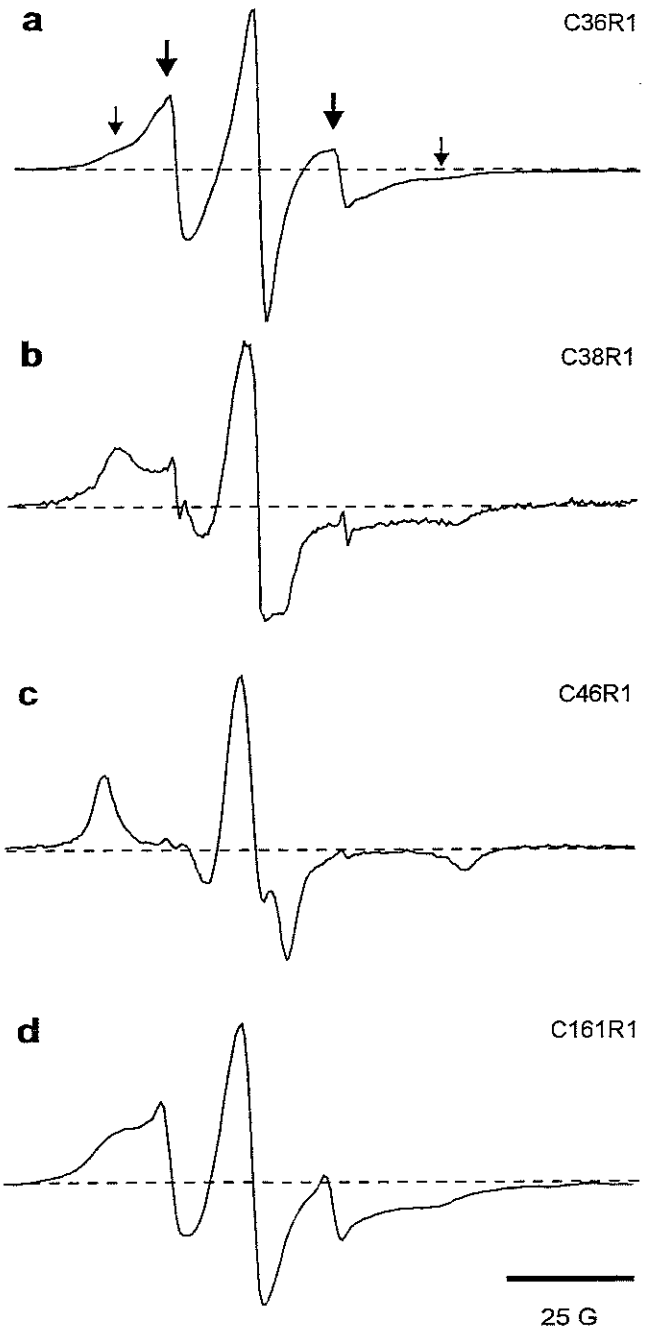

FIGURE 2 Continuous-wave EPR spectra of the spin-label MTSSL attached to (*a*) D36C, (*b*) D38C, (*c*) T46C, and (*d*) E161C. The arrows in *a* indicate the spectral components due to the mobile (*large arrows*) and more immobile (*small arrows*) fractions of the nitroxides.

EPR spectra of spin-labeled BR mutants, in which the cysteines are located on the outer surface of the helices or are attached to interhelical loops (Altenbach et al., 1990; Greenhalgh et al., 1991; Altenbach et al., 1994), the mobile part of the spectrum of C36R1 shows the highest degree of mobility of the R1 side chain, with a reorientation correlation time of the nitroxide of 3 ns. Similarities can be found to the spectral shape of C74R1 (Greenhalgh et al., 1991) in BR-containing liposomes and to that of C72R1 in detergent-solubilized BR (Altenbach et al., 1989). Both mutations are located in the B-C interhelical loop at the extracellular surface of the protein, and the high degree of spin label mobility has only been found in protein preparations, where intermolecular interaction or local constraints are removed. Thus the present high mobility of the C36R1 side chain in the BR-trimer is a result of negligible intermolecular and intramolecular contacts. This may be due to the location of C36R1 close to the center of the A-B interhelical loop, with the small amino acid side chains of serine and proline being the nearest neighbors, and argues in favor of an orientation of the R1 side chain pointing away from the protein center (cf. Fig. 1, *b* and *c*; Grigorieff et al., 1996). The amplitude ratio of the two spectral components changes within 2 weeks after spin labeling in favor of a more restricted motion of R1. This may indicate a very slow structural change in the purple membrane that enhances the interaction of the nitroxide with its environment, e.g., with atoms of helix D of a neighboring molecule in the trimer (Fig. 1 *c*).

The spectra of C38R1, C46R1, and C161R1 (Fig. 2 *b–d*) reflect a restricted motion of R1. The spectra of C38R1 and C161R1 could be fitted with reorientation correlation times of the nitroxide of 10 ns and 5 ns, respectively. The spectral shapes are similar to those found for C101R1 or C105R1 in the C-D interhelical loop (Steinhoff et al., 1994). This slow motion of the nitroxides is a result of their interaction with the neighboring secondary and tertiary structure and is evidence for a structured region in the nitroxide environment. The spectral shape of C46R1 shows a very high immobilization of the nitroxide side chain, which is typical of spin labels located in the interior of a protein (Altenbach et al., 1990). Here the motional cone of the nitroxide ring is restricted because of multiple interaction with neighboring side-chain and backbone atoms.

Absorbance changes in the visible spectrum during the photocycle

Absorbance changes after photoexcitation were measured in the visible spectrum at 11 wavelengths, as described in Materials and Methods. With an experimental sampling time of 0.2 ms, the global fit analysis yields four time constants for the samples measured at pH 7.4, and five constants for the sample measured at pH 10 in 3 M KCl. Because of the chosen time resolution, the early intermediates of the photocycle and the biphasic rise of M (Hessling et al., 1993) are not resolved. The absorbance band of M at 410 nm rises with a time constant of less than 0.2 ms. The apparent time constants describing the M decay and the kinetics of the following intermediates are numbered according to other authors (Hessling et al., 1993). At pH 7.4, the M intermediate decays with three time constants, τ_4, τ_3, and τ_6. The data of these time constants are given in Table 1. With the exception of D38C and C38R1, the values of τ_4 are the same within a factor of 2 for wild-type BR and all mutants. Compared to the wild-type protein, the values of τ_3 are higher by a factor of 2–6, and the values of τ_6 increased 10- to 15-fold, again with the exception of D38C and C38R1. A significant increase in τ_4 and τ_3, as well as a dramatic increase in τ_6, compared to the other samples is found for D38C. Considering the slightly different pH and buffer composition, our results agree with the data published by Riesle et al. (1996). Spin labeling of the cysteines of the mutants does not further change the rates significantly. The sample C36R1 was also studied in 3 M KCl at pH 10.0. An additional time constant, τ_7, is required to describe the M-decay. Compared to the same sample at pH 7.4, the values of the time constants τ_3 and τ_6 are increased by a factor of 15.

TABLE 1 Time constants* for the second half of the photocycle, determined by global fit analysis of the absorbance changes in the visible spectrum between 405 nm and 665 nm, and of the EPR transient signal changes

	WT#	D36C	C36R1		D38C	C38R1	T46C	C46R1		E161C	C161R1	
	VIS	VIS		EPR	VIS		VIS		EPR	VIS		EPR
τ_4/ms	2.2	2.0	3.5 (2.4)	2.2 (2.4)§	8	4.8	4.3	5.1	3.7	4.1	4.1	<0.5
τ_3/ms	7.0	14	18 (330)	18 (330)§	58	46	27	42	40	26	23	20
τ_6/ms	18	170	170 (2600)	140 (2300)	830	670	170	290	240	270	190	200
τ_7/ms			(29)	(29)§								

The values for C36R1 in suspension at pH 10.0 are given in parentheses.

*Standard deviations of the time constants determined in the visible are less than 10%. The respective standard deviations for the values determined from the EPR transients are less than 15%.

#Wild-type BR.

§EPR transients included in global fit with optical data.

The amplitude spectra of the apparent time constants of the unlabeled and the spin-labeled samples show a quite similar behavior. Therefore, only the spectra of the spin-labeled samples are shown in Fig. 3. These amplitude spectra are mixtures of difference spectra between the BR ground state and the different intermediates. The time constant τ_4 describes the decay of a fraction of intermediate M, and the rise of the intermediates N, O, and a fraction of the BR ground state: the spectral amplitudes at the absorbance maxima of N (550 nm), BR (570 nm), and O (660 nm) are negative. Because of the partial overlap of the absorbance bands of the N state and that of the BR ground state, a quantitative discrimination between these two states is difficult. However, the rise of the N intermediate with τ_4 is pronounced for C36R1 at pH 10.0 (Fig. 3 *b*), where the amplitude spectrum reveals its minimum value at 550 nm. The decay of the remaining fractions of M, N, and O is determined by τ_3 and τ_6. Whereas the significant contribution of O to the τ_3 amplitude spectrum is revealed by the positive amplitude at 660 nm for C36R1 (pH 7.4) and C161R1, this contribution is hardly observed for C36R1 (pH 10), C38R1, and C46R1. The fraction of the intermediate O found for wild-type BR at pH 6.5, T = 298 K, is significantly higher than those found here for C36R1 and C161R1, but the respective value determined at pH 7.5 and T = 288K agrees well with the data shown in Fig. 3, *a* and

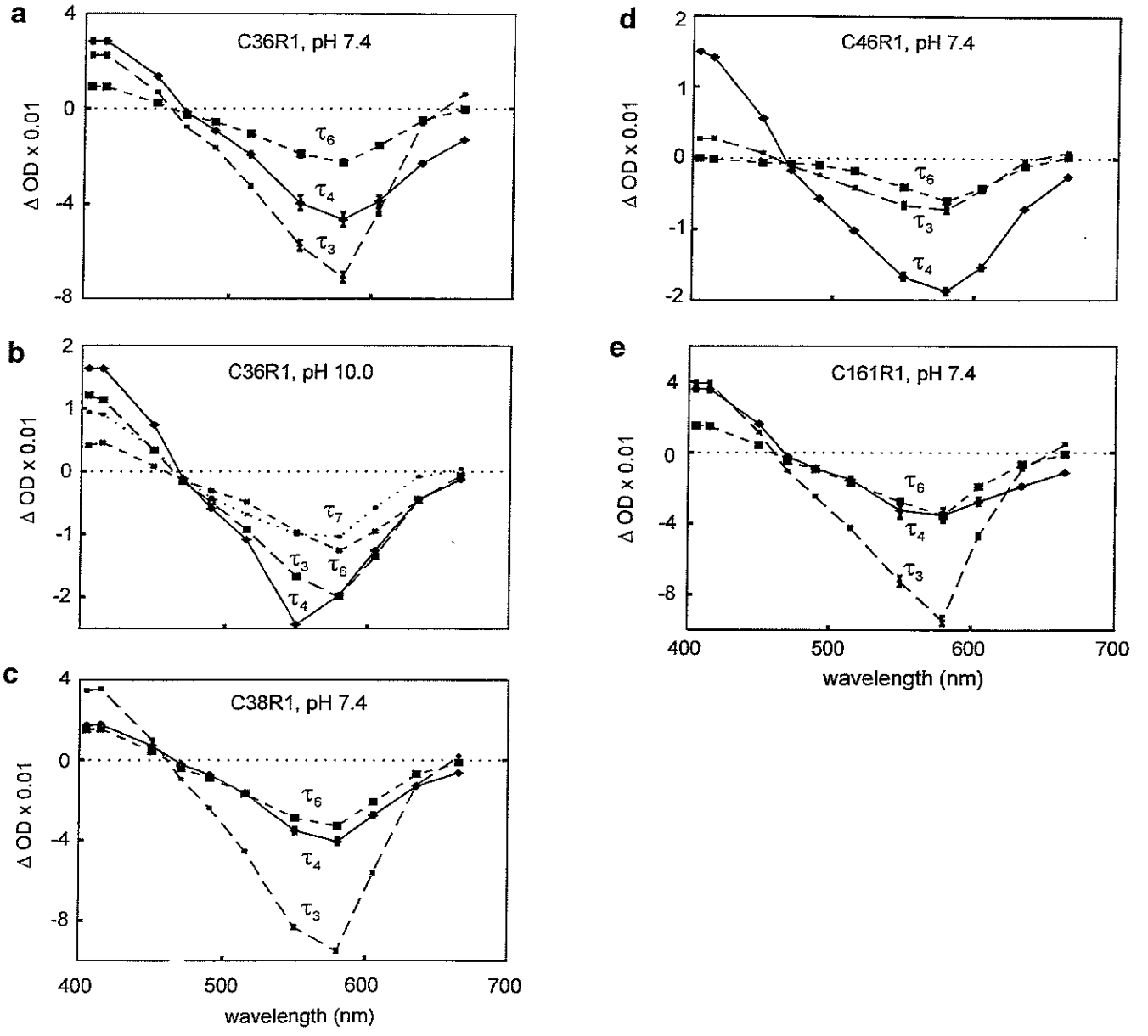

FIGURE 3 Amplitude spectra of the apparent time constants describing the absorbance changes in the visible spectrum at pH 7.4, T = 293K in 0.1 M NaCl. C36R1 was studied further at pH 10.0 in 3M KCl. (*a*) C36R1; (*b*) C36R1, pH 10, 3 M KCl; (*c*) C38R1; (*d*) C46R1; (*e*) E161R1. Those data points without error bars have standard deviations smaller than the symbol size. The values of the corresponding time constants are given in Table 1.

e (Hessling et al., 1993). The τ_6 amplitude spectrum exhibits mainly a mixture of the BR-M and BR-N difference spectra for all mutants. Because of the overlap of the absorbance bands of N (550 nm) and BR (570 nm), the contributions of N to the τ_3 and τ_6 amplitude spectra are not as obvious as those of M and O. As is the case for τ_4, the additional time constant τ_7 describes the M-to-N transition for C36R1 at pH 10. The behavior of the amplitude spectra of C36R1 and C161R1 resembles that found for the wild-type BR measured at pH 7.5 (Souvignier and Gerwert, 1992; Hessling et al., 1993). However, the fraction of at least the O intermediate seems to be very low for C38R1 and C46R1. The accumulation of the N intermediate associated with the increase of its lifetime at alkaline pH found for C36R1 agrees well with results reported for wild-type BR (Maeda et al., 1986). Therefore, we conclude that the time constants characterizing the M-decay of all but one sample (D38C) are increased slightly after the exchange of the natural amino acids by cysteines. This may be due to the charge changes on the cytoplasmic surface of the BR molecule or, as in the case of T46C, changes in the hydrogen network or a steric modification in the interior of the protein (Rothschild et al., 1992; Coleman et al., 1995; LeCoutre et al., 1996). The most dramatic change is found for D38C, in which the photocycle is retarded close to values known from D96 mutants (Riesle et al., 1996). Otherwise, spin labeling of the cysteines does not influence the photocycle; thus further significant distortion of the structure and function of BR by the attached spin labels is unlikely.

EPR spectral changes induced by photoactivation

Changes in the EPR spectra caused by photoexcitation were monitored at discrete values of the magnetic field. Transient EPR signal changes were observed for C36R1, C46R1, and C161R1, whereas the spectrum of C38R1 did not show any transient changes above noise. The relative values of the transient EPR amplitude changes determined 10 ms after the laser flash are given in Fig. 4, *a*, *d*, and *g*, for selected B-field values. The maximum transient signals of C36R1 and C161R1 amount to ~20% of the maximum amplitude changes detected for C46R1. These values are similar to those found for C101R1 under the present experimental conditions. To determine whether these EPR spectral changes were due to transient changes in the nitroxide mobility or to changes in the polarity in the nitroxide environment, spectral simulations were performed and compared with the experimental data. The derivatives of the EPR spectra $S(B)$ with respect to the reorientation correlation time, $dS/d\tau$, and with respect to the values of the hyperfine coupling constant, dS/dA_{zz}, which is a measure of the polarity in the environment of the nitroxide, were determined numerically by using Freed's program for EPR spectra simulations (Freed, 1976; Schneider and Freed, 1989). ($S(B)$ denotes the usually detected EPR spectrum, which is the first-derivative absorption spectrum with respect to B.) The simulations are shown in Fig. 4. Because of the high mobility of the C36R1 side chain, the derivatives of

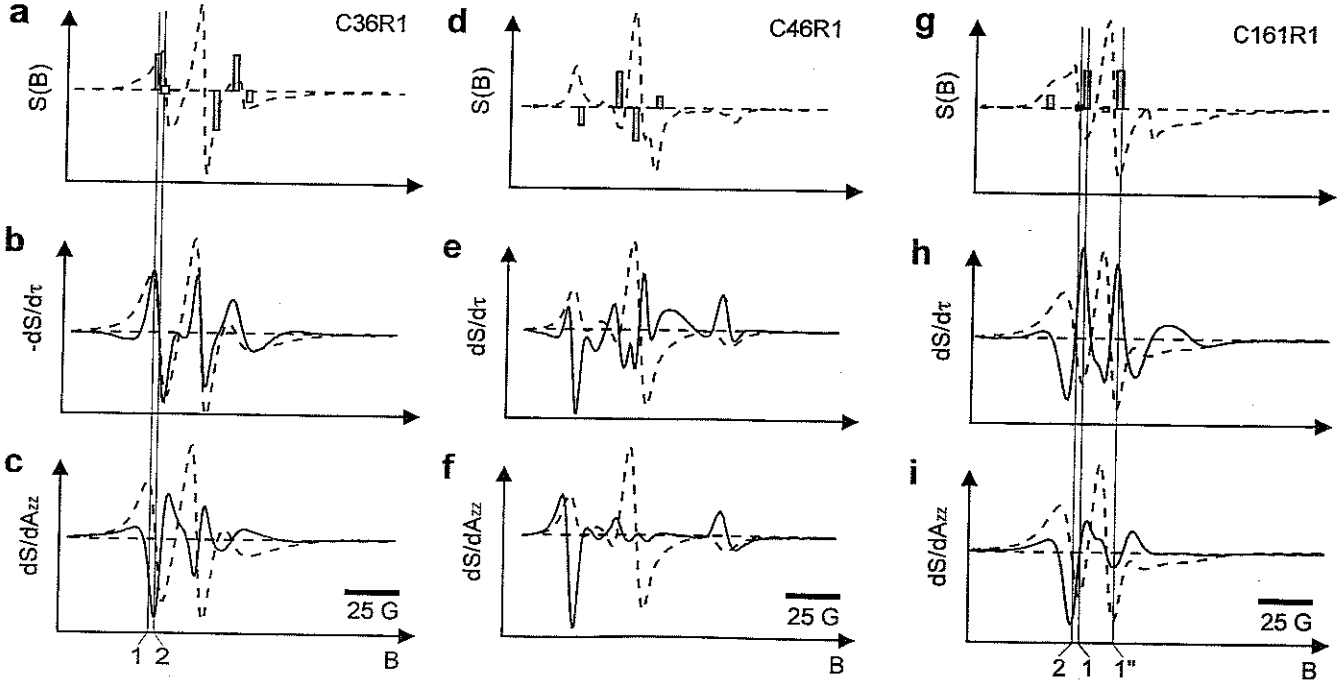

FIGURE 4 Relative amplitudes of the spectral changes (*bars*) detected at selected B-field values 10 ms after the initiation of the photocycle for (*a*) C36R1, (*d*) C46R1, and (*g*) C161R1. Compared to the amplitude of the cw-EPR spectrum (*dashed lines*), the bars are magnified by a factor of 50 in *a* and *g* and by a factor of 10 in *d*. Simulations of EPR spectra (*dashed lines*) and spectral changes (*solid lines*) due to changes in the nitroxide mobility, ($dS/d\tau$), are shown in *b*, *e*, and *h* for the respective mutants. Spectra and spectral changes due to changes in the environmental polarity, (dS/dA_{zz}), are given in *c*, *f*, and *i*. The vertical dashed lines indicate spectral positions with maximum spectral sensitivity due to mobility changes (1, 1") or polarity changes (2).

the EPR spectra with respect to the correlation time, $dS/d\tau$, and with respect to the hyperfine splitting, dS/dA, show structures with small line widths (Fig. 4, *b* and *c*). An increase in the nitroxide mobility (i.e., a decrease in the reorientation correlation time) leads to an increase in the EPR spectral amplitude in the first maximum of the spectrum (*B*-field position 1 in Fig. 4 *b*). At this *B*-field value, the derivative with respect to the hyperfine coupling constant is small (cf. Fig. 4 *c*). The contrary is true at *B*-field positon 2. Here the derivative with respect to the correlation time is zero (Fig. 4 *b*), and the derivative with respect to a polarity change reveals its maximum negative amplitude (Fig. 4 *c*). The experimentally determined amplitude at *B*-field position 2 is zero. Thus the comparison of the observed spectral changes with the simulations demonstrates that the transient EPR signals must be due to a transient increase in the nitroxide mobility of C36R1. The other three transient signals shown in Fig. 4 *a* are in agreement with the above conclusion. For C36R1 samples with a changed amplitude ratio of mobile to immobile component, the EPR spectral changes indicate a transient decrease in the nitroxide mobility.

The experimentally observed transient amplitudes of C161R1 and the simulated derivatives with respect to the change in the mobility and in the polarity are shown in Fig. 4, *g*, *h*, and *i*. The transient amplitudes detected at the low-field and center-field minimum positions (*B*-field positions 1 and 1″) indicate a transient mobility change in the nitroxide (Fig. 4 *h*). The transient amplitude changes do not agree with the spectral changes expected for a polarity change, which should be at maximum at *B*-field position 2 (Fig. 4 *i*). Thus the amplitudes and signs of the transients clearly argue in favor of a transient increase in the rotational correlation time, i.e., a decrease in the mobility of the attached nitroxide during the last half of the photocycle.

For very immobilized nitroxides with apparent rotational correlation times of more than 20 ns (as is found for the spin label attached to T46C), the spectral derivates with respect to τ and A_{zz} are very similar in the low-field and high-field regions (Fig. 4, *e* and *f*). The experimentally observed large-amplitude changes in the center line (Fig. 4 *d*), however, indicate a transient decrease in mobility. To clearly separate motional effects from polarity influences on the shape of the EPR spectral changes, an independent method has been used for C46R1. After the photocycle of C46R1 has been stopped by freezing at different temperatures in the range between 170 K and 270 K, the hyperfine tensor values were determined at low temperature (T = 170 K). The A_{zz} values were found to be independent of the different fractions of intermediates accumulated by the freezing procedure. The value of A_{zz} amounts to 34.7 ± 0.1 Gauss in the whole temperature range. Thus, there is no evidence that a significant change in the polarity in the vicinity of the nitroxide group is responsible for the spectral changes observed during the photocycle.

The time dependence of the EPR signal was recorded at the indicated magnetic field values to correlate the light-induced EPR spectral changes with the observed absorbance changes in the visible spectrum. Typical EPR transients for C36R1, C46R1, and C161R1 are shown in Fig. 5, together with optical transients measured at 410 nm. The time resolution of the present EPR experiments is mainly limited by the signal-to-noise ratio. Data acquisition started 0.2 ms after the light flash; however, only data for times exceeding the detector time constant were used to fit the data shown in the figure. The EPR transient signals for C36R1 (cf. Fig. 5, *a* and *b*) and C46R1 (cf. Fig. 5 *c*) appear during the decay of the M intermediate and reverse with the recovery of the BR ground state. The rise of the EPR transient signal for C161R1 (cf. Fig. 5 *d*) could not be fully resolved. The observed spectral change is already present after the appearance of M. The EPR signal changes of each mutant determined for four magnetic field values were fitted to a sum of exponential functions. The resulting kinetic parameters are given in Table 1; the calculated curves are shown in Fig. 5. The EPR signals of C36R1 and C46R1 rise with a time constant similar to the fastest M-decay time detected in the visible spectrum (τ_4). The respective rise time of C161R1 is less than 0.5 ms. The decay of the EPR transient signals of C36R1 and C161R1 is dominated by the time constant τ_3. The contribution of τ_6 to the decay amplitude is ~30%. The time constants determined from the EPR transients agree with the respective values measured in the visible spectrum. The EPR transient signals of C46R1 and C36R1, pH 10, are governed by τ_4, which describes the signal rise. The largest time constant measured in the visible spectrum, τ_6, characterizes the EPR signal decay. The contribution of τ_3 to the decay amplitude and that of τ_7 to the signal rise for C36R1, pH 10, amount to less than 20%. Within experimental error, all time constants agree with those measured in the visible spectrum (cf. Table 1).

DISCUSSION

Although a fairly detailed picture exists of the proton pathway through bacteriorhodopsin, including the specific role of certain amino acid side chains revealed by FTIR spectroscopy, the characteristics and the mechanism of the structural changes during the photocycle are still obscure.

Rearrangement of the membrane-embedded α-helices and of the cytoplasmic loops may correspond to a switch that makes the Schiff base accessible from the extracellular medium (Oesterhelt et al., 1992). The complete description of these structural changes with high local and time resolutions would be the first example of a detailed understanding of such a switch, which is an essential element of all vectorial catalytic mechanisms. Diffraction studies (Koch et al., 1991; Subramaniam et al., 1993) followed a conformational change that occurs during the lifetime of the M intermediate and decays with the N intermediate. Conformational changes of the BR backbone were also concluded from amide band changes observed by FTIR spectroscopy (Souvignier and Gerwert, 1992; Rothschild et al., 1993;

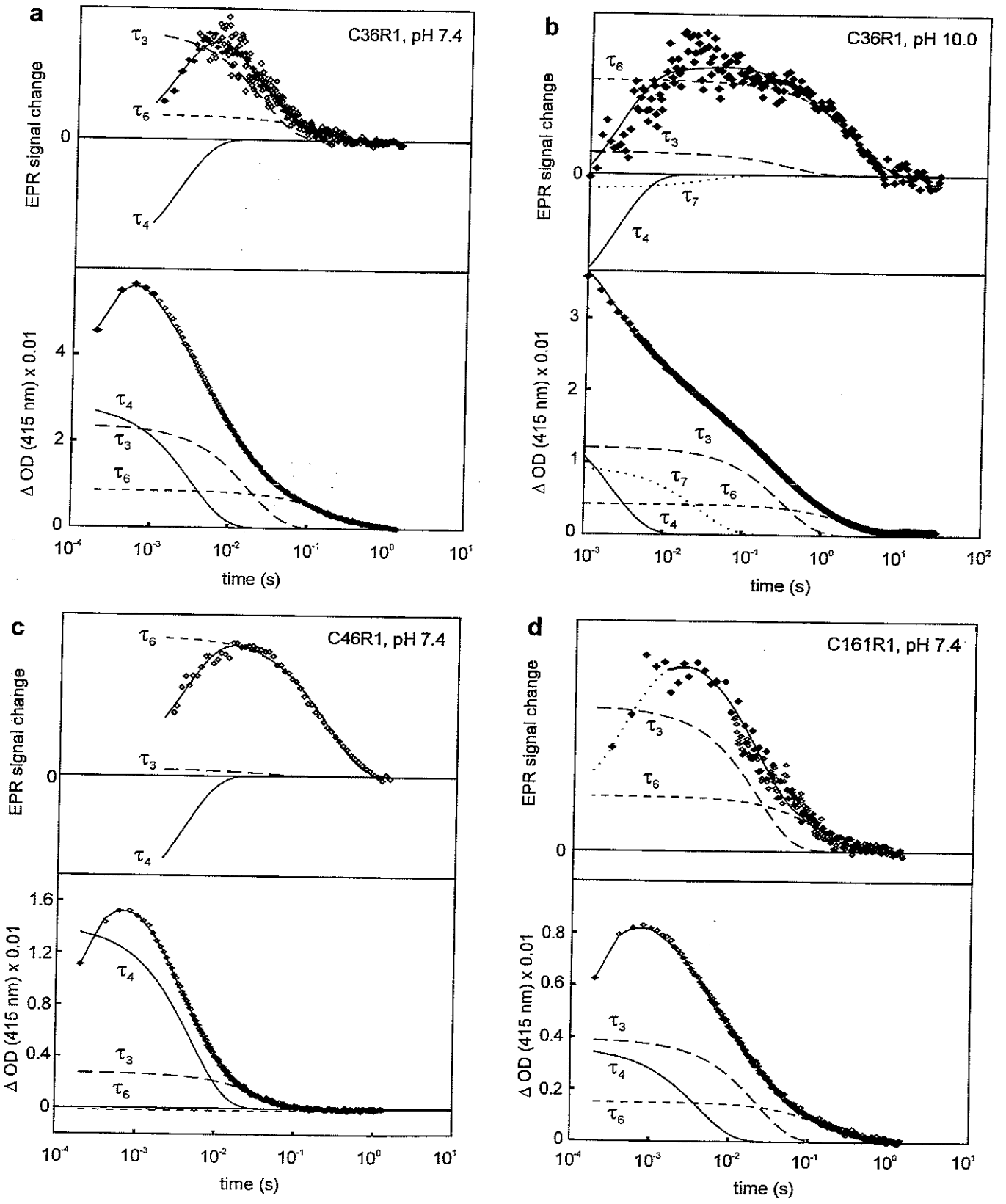

FIGURE 5 EPR signal changes and absorbance changes after photoexcitation monitored at 415 nm. Exponential fit curves and the contributions of the dominating time constants are included. (*a*) C36R1; (*b*) C36R1 in 3 M KCl, pH 10.0; (*c*) C46R1; and (*d*) C161R1. Two experimental EPR transient signals with total sampling ranges from 1 ms to 200 ms (◆) and from 3 ms to 2 s (◇) are shown in *a*. The respective ranges in *b* are 1 ms to 6 s and 6 s to 30 s, and those in *d* are 0.2 ms to 200 ms and 10 ms to 2 s.

Hessling et al., 1993). The largest peptide backbone movements appear during the M-to-N transition. EPR experiments with a spin label attached to a cysteine in the cytoplasmic C-D loop of the bR mutant V101C revealed spectral changes during the photocycle, which rise after the appearance of the M intermediate and decay with the recovery to the BR ground state (Steinhoff et al., 1994). These spectral changes were interpreted as structural rearrangements near D96 or as a structural change in the E-F interhelical loop. However, the detailed characterization and understanding of the movement of the helical and loop structures is still a central question.

We used the site-directed spin-labeling technique to investigate possible structural rearrangements in the interhelical loops A-B (C36R1, C38R1) and E-F (C161R1) and in the interior of the protein in the vicinity of D96 (C46R1). The apparent time constants that describe the second half of the photocycle of the mutants D36C, T46C, and D161C are similar to the respective values found for the spin-labeled samples C36R1, C46R1, and C161R1. The values found for the time constants τ_4, which describe the M-to-N and M-to-O transitions, and for τ_3, which characterizes the decay of M and O, are similar to or slightly higher than the respective values measured for wild-type BR at pH 7.4. However, the value of τ_6 is significantly increased by an order of magnitude compared to that of the wild type. The analysis of the amplitude spectra (Fig. 3) and FTIR experiments on wild-type BR combined with factor analysis demonstrated that τ_6 characterizes the decay of the N intermediate (Hessling et al., 1993). This step involves the reprotonation of D96 from the cytoplasmic surface. The increase in the lifetime of the N intermediate for the mutation at positions 36 and 161 may be caused by the delay of the proton transport to D96 due to the lack of proton donor side chains in the mutants. A further increase in the lifetime of the N intermediate for C36R1 at high pH results from the lack of protons in the solution, which slows down the reprotonation rate of D96 (Maeda et al., 1986). A dramatic 50-fold increase in the photocycle lifetime is found for D38C. This is in agreement with the results of Riesle et al. (1996), who concluded that D38 is involved in the proton transport pathway on the cytoplasmic surface of BR.

The influence of the C46R1 mutation on the photocycle may be due to the close proximity of position 46 to D96, as shown by the structure model determined by electron diffraction (Henderson et al., 1990; Grigorieff et al., 1996) (see Fig. 1 *b*). Several studies indicate that T46 interacts with D96 (Marti et al., 1991; Rothschild et al., 1992; Brown et al., 1994; Coleman et al., 1995) and may be part of a hydrogen network between the cytoplasmic surface and the Schiff base (LeCoutre et al., 1996). The mutation at position 46 may thus influence the accessibility of D96 for the proton delivered by the cytoplasmic medium, which may result in the observed delay of the N decay.

The degree of the nitroxide mobility determined from the continuous-wave EPR spectral shape of the mutants C36R1, C38R1, and C161R1 is consistent with previous studies in which MTSSL was attached to sites in interhelical loops (Altenbach et al., 1990; Steinhoff et al., 1994). A component of very high mobility is found for the spin label attached to C36, which indicates minor secondary and tertiary interaction with the environment. This agrees with the structural data (Grigorieff et al., 1996) (cf. Fig. 1 *b*). The high degree of immobilization of the spin label attached to position 46 is due to the interaction of the nitroxide side chain with the densely packed side chain and backbone atoms in its vicinity, as shown by molecular graphics analysis based on the structural model (cf. Fig. 1, *b* and *c*). The EPR spectrum is similar to those found for MTSSL attached to positions where the spin-label side chain is known to point into the interior of the protein (Altenbach et al., 1990).

Upon photoexcitation, EPR transients are detectable for C36R1, C161R1, and C46R1. No mobility changes are observed for the nitroxide side chain attached to C38, which agrees with FTIR experiments and electron diffraction studies, where no significant conformational change during the photocycle was detected (Riesle et al., 1996). The rise time of the transient EPR signal of C161R1 in the E-F loop was estimated to be less than 0.5 ms. Thus the observed environmental change in the vicinity of position 161 already occurs during the lifetime of the M intermediate. In contrast, the small transient spectral changes of the nitroxides attached within the A-B loop, C36R1, rise with a time constant that agrees with the M-to-N transition, as determined from spectral analysis in the visible spectrum (τ_4). The EPR transient signals decay with time constants found for the decays of the M and N intermediates in the visible spectrum (τ_3 and τ_6). The appearance of a conformational change during the lifetime of the M intermediate, which might be responsible for the mobility change of the spin label in the mutant C161R1, agrees with the interpretation of electron and x-ray diffraction data. In wild-type BR, electron diffraction studies reveal a significant ordering of helix G and minor changes close to helices B, C, and F that occur in the M state (Subramaniam et al., 1993). The structures were found to be similar under experimental conditions where either the M or the N state should predominate. From this the authors conclude that the observed structural changes are involved in the proposed M_1-to-M_2 transition. X-ray diffraction and FTIR studies on wild-type BR and on the mutant D96N at different degrees of hydration point also to the existence of distinct states in the M intermediate that differ in their conformation (Sass et al., 1997). The transient mobility change of the nitroxide attached to C161 in the E-F loop may be the consequence of these conformational changes close to helices F or C observed in the diffraction difference maps. However, the EPR spectral changes detected for the nitroxide attached to the A-B loop, C36R1, and to helix B, C46R1, rise with a time constant, τ_4, found for the M-to-N transition. Because the spectral analysis in the visible spectrum cannot discriminate between the proposed M_1 and M_2 intermediates, it is not clear whether τ_4 describes the M_2-to-N transition or mainly the M_1-to-N transition, because of a very fast M_2 decay. However, FTIR

studies in combination with double-flash experiments resolve two different M intermediates, which are identified with M_1 and M_2. The transition between these two intermediates is fast compared to the M_2-to-N transition (Hessling, 1996; Hessling et al., manuscript submitted for publication). Thus τ_4 is expected to characterize the M_2-to-N transition. During this transition, significant changes occur in the environment of the attached spin labels that are not resolved in the diffraction pattern. This may be due to the fact that the structural changes resolved by EPR at position 36 or 46 are not sufficiently large to be detectable by diffraction methods with the resolution available at present. The appearance of structural rearrangements after the formation of M and during the M-to-N transition corresponds to conclusions from FTIR data. These experiments indicate the presence of only small protein movements in the M_1-to-M_2 transition and larger structural changes in the M-to-N transition (Hessling et al., 1993; Hessling et al., manuscript submitted for publication). These changes may reflect the protein motions that lead to an increase of the nitroxide mobility for the mobile nitroxide fraction of C36R1, and to a contrary behavior for the more immobile fraction of C36R1 in the A-B loop and for C161R1 in the E-F loop.

What kind of protein movement could account for the above results? The mobility of an attached nitroxide is determined by the residual motion of the spin label with respect to the backbone. The degree of interaction of the nitroxide with atoms of the neighboring side chains and backbone determines the restriction of its reorientational motion (Hubbell and Altenbach, 1994). In addition, protein fluctuations and the intrinsic local flexibility of the peptide chain the nitroxide is attached to are reflected in the EPR spectral shape (Steinhoff et al., 1989; Miick et al., 1991; Todd and Millhauser, 1991). Thus the changes in the nitroxide mobility of C36R1 indicate changes in secondary or tertiary interactions in the A-B loop during the M-to-N transition. The changes in the spin label dynamics of C161R1 reflect changes in the environment of the E-F loop during the M formation or the proposed M_1-to-M_2 transition.

The rearrangement of the hydrogen-bonded network with a transient increase in the polarity in the vicinity of the nitroxide oxygen during the N intermediate is unlikely to account for the data of C46R1. The direction of the EPR signal change is consistent, however, with a decrease in the motional freedom of the nitroxide during the N intermediate due to structural changes in the vicinity of the spin-label binding site. The results of electron diffraction studies suggest that a movement of the cytoplasmic segments of helices B, C, and F and a transient ordering of helix G occur during the M intermediate and reverse with the recovery of the BR ground state (Subramaniam et al., 1993). These helix movements might lead to rearrangements of the A-B and E-F loops with changed intrinsic flexibilities. An increase in the local flexibility of the A-B loop and a contrary behavior of the E-F loop would account for our data. Inspection of possible locations of the R1 side chain of C46R1 reveal interactions with helices G and F (cf. Fig. 1, *b* and *c*). An easy explanation for the increased motional constraint of the R1 side chain in the C46R1 mutant during the N intermediate is that a rearrangement of helix G leads to an increased interaction between the nitroxide and the adjacent side-chain or backbone atoms.

In summary, our results indicate that small structural rearrangements of the E-F loop and the A-B loop occur during the M intermediate and during the M-to-N transition, respectively. These changes in the environment of the spin-label binding sites reverse with the N decay. However, the most prominent mobility changes in the attached nitroxides are detected at positions 46 and 101 (Steinhoff et al., 1994). The side chain of C101R1 is located at the cytoplasmic side and that of C46R1 at the extracellular side with respect to D96 (cf. Fig. 1 *b*). The time-resolved nitroxide mobility changes reflect the rearrangement of amino acid residues in the proximity of D96 during the N intermediate of the photocycle.

We gratefully acknowledge the support of the Deutsche Forschungsgemeinschaft Ste640-2/1 and SFB 394, C1 and C2 (TR, KG, and H-JS).

REFERENCES

Altenbach, C., S. L. Flitsch, H. G. Khorana, and W. L. Hubbell. 1989. Structural studies on transmembrane proteins. 2. Spin labeling of bacteriorhodopsin mutants at unique cysteines. *Biochemistry.* 28: 7806–7812.

Altenbach, C., D. Greenhalgh, H. G. Khorana, and W. L. Hubbell. 1994. A collison gradient method to determine the immersion depth of nitroxides in lipid bilayers: application to spin-labeled mutants of bacteriorhodopsin. *Proc. Natl. Acad. Sci. USA.* 91:1667–1671.

Altenbach, C., T. Marti, H. G. Khorana, and W. L. Hubbell. 1990. Transmembrane protein structure: spin labeling of bacteriorhodopsin mutants. *Science.* 248:1088–1092.

Braiman, M. S., T. Mogi, T. Marti, L. J. Stern, H. G. Khorana, and K. J. Rothschild. 1988. Vibrational spectroscopy of bacteriorhodopsin mutants: light-driven proton transport involves protonation changes of aspartic acid residues 85, 96, and 212. *Biochemistry.* 27:8516–8520.

Brown, L. S., Y. Yamazaki, A. Maeda, L. Sun, R. Needleman, and J. K. Lanyi. 1994. The proton transfers in the cytoplasmic domain of bacteriorhodopsin are facilitated by a cluster of interacting residues. *J. Mol. Biol.* 239:401–414.

Coleman, M., A. Nilsson, T. S. Russell, P. Rath, R. Pandey, and K. J. Rothschild. 1995. Asp 46 can substitute for asp 96 as the Schiff base proton donor in bacteriorhodopsin. *Biochemistry.* 34:15599–15606.

Ferrando, E., U. Schweiger, and D. Oesterhelt. 1993. Homologous bacterio-opsin-encoding gene expression via site-specific vector integration. *Gene.* 125:41–47

Freed, J. H. 1976. Theory of slow tumbling ESR spectra of nitroxides. *In* Spin Labeling Theory and Applications. L. J. Berliner, editor. Academic Press, New York. 53–132.

Gerwert, K., B. Hess, J. Soppa, and D. Oesterhelt. 1989. Role of aspartate-96 in proton translocation by bacteriorhodopsin. *Proc. Natl. Acad. Sci. USA.* 86:4943–4947.

Gerwert, K., and F. Siebert. 1986. Evidence for light-induced 13-*cis*, 14-s-*cis* isomerization in bacteriorhodopsin obtained by FTIR difference spectroscopy using isotopically labelled retinals. *EMBO J.* 5:805–811.

Gerwert, K., G. Souvignier, and B. Hess. 1990. Simultaneous monitoring of light-induced changes in protein side group protonation, chromophore isomerization and backbone motion of bacteriorhodopsin by time-resolved Fourier-transform infrared spectroscopy. *Proc. Natl. Acad. Sci. USA.* 87:9774–9778.

Greenhalgh, D., C. Altenbach, W. L. Hubbell, and H. G. Khorana. 1991. Locations of Arg-82, Asp-85, and Asp-96 in helix C of bacteriorhodopsin relative to the aqueous boundaries. *Proc. Natl. Acad. Sci. USA.* 88:8626–8630.

Grigorieff, N., T. A. Ceska, K. H. Downing, J. M. Baldwin, and R. Henderson. 1996. Electron-crystallographic refinement of the structure of bacteriorhodopsin. *J. Mol. Biol.* 259:393–421.

Henderson, R., J. M. Baldwin, T. A. Ceska, F. Zemlin, E. Beckmann, and K. H. Dowing. 1990. Model for the structure of bacteriorhodopsin based on high-resolution electron cryo-microscopy. *J. Mol. Biol.* 213: 899–929.

Hessling, B. 1996. Vibrationsspektroskopische Untersuchungen zum Reprotonierungsschritt der zentralen Protonenbindungsstelle im Photozyklus von Bakteriorhodopsin. Dissertation. Ruhr-Universität Bochum.

Hessling, B., G. Souvignier, and K. Gerwert. 1993. A model-independent approach to assigning bacteriorhodopsin's intramolecular reactions to photocycle intermediates. *Biophys. J.* 65:1929–1941.

Hubbell, W. L., and C. Altenbach. 1994. Investigation of structure and dynamics in membrane proteins using site-directed spin labeling. *Curr. Opin. Struct. Biol.* 4:566–573.

Kataoka, M., H. Kamikubo, F. Tokunaga, L. S. Brown, Y. Yamazaki, A. Maeda, M. Sheves, R. Needleman, and J. Lanyi. 1994. Energy coupling in an ion pump. The reprotonation switch of bacteriorhodopsin. *J. Mol. Biol.* 243:621–638.

Koch, M. H. J., N. A. Dencher, D. Oesterhelt, H.-J. Plön, G. Rapp, and G. Büldt. 1991. Time-resolved x-ray diffraction study of structural changes associated with the photocycle of bacteriorhodopsin. *EMBO J.* 10: 521–526.

Lanyi, J. K. 1993. Proton translocation mechanism and energetics in the light-driven pump bacteriorhodopsin. *Biochem. Biophys. Acta.* 1183: 241–261.

LeCoutre, J., J. Tittor, D. Oesterhelt, and K. Gerwert. 1996. Experimental evidence for hydrogen-bonded network proton transfer in bacteriorhodopsin shown by Fourier-transform infrared spectroscopy using azide as catalyst. *Proc. Natl. Acad. Sci. USA.* 92:4962–4966.

Lozier, R. H., A. Xie, J. Hofrichter, and G. M. Clore. 1992. Reversible steps in the bacteriorhodopsin photocycle. *Proc. Natl. Acad. Sci. USA.* 89:610–614.

Maeda, A., T. Ogura, and T. Kitagawa. 1986. Resonance Raman study on proton-dissociated state of bacteriorhodopsin: stabilization of L-like intermediate having the all-*trans* chromophore. *Biochemistry.* 25: 2798–2803.

Marti, T., H. Otto, T. Mogi, S. J. Rösselet, M. P. Heyn, and H. G. Khorana. 1991. Bacteriorhodopsin mutants containing single substitutions of serine or threonine residues are all active in proton translocation. *J. Biol. Chem.* 266:6919–6927.

Maurer, R., J. Vogel, and S. Schneider. 1987. Analysis of flash photolysis data by a global fit with multi-exponentials. I. Determination of the minimal number of intermediates in the photocycle of bacteriorhodopsin by the stability criterion. *Photochem. Photobiol.* 46:247–253.

Miick, S. M., K. M. Casteel, and G. L. Millhauser. 1993. Experimental molecular dynamics of an alanine-based helical peptide determined by spin label electron spin resonance. *Biochemistry.* 32:8014–8021.

Miick, S. M., A. P. Todd, and G. L. Millhauser. 1991. Position-dependent local motions in spin-labeled analogues of a short α-helical peptide determined by electron spin resonance. *Biochemistry.* 30:9498–9503.

Nakasako, M., M. Kataoka, Y. Amemiya, and F. Tokunaga. 1991. Crystallographic characterization by X-ray diffraction of the M-intermediate from the photo-cycle of bacteriorhodopsin at room temperature. *FEBS Lett.* 292:73–75.

Oesterhelt, D., and W. Stoeckenius. 1974. Isolation of the cell membrane of *Halobacterium halobium* and its fraction into red and purple membrane. *Methods Enzymol.* 31:667–686.

Oesterhelt, D., J. Tittor, and E. Bamberg. 1992. A unifying concept for ion translocation by retinal proteins. *J. Bioenerg. Biomembr.* 24:181–191.

Riesle, J., D. Oesterhelt, N. A. Dencher, and J. Heberle. 1996. D38 is an essential part of the proton translocation pathway in bacteriorhodopsin. *J. Biol. Chem.* 35:6635–6643.

Rothschild, K., Y.-W. He, S. Sonar, T. Marti, and H. G. Khorana. 1992. Vibrational spectroscopy of bacteriorhodopsin mutants. *J. Biol. Chem.* 267:1615–1622.

Rothschild, K. J., T. Marti, S. Sonar, Y.-W. He, P. Rath, W. Fischer, and H. G. Khorana. 1993. Asp 96 deprotonation and transmembrane α-helical structural changes in bacteriorhodopsin. *J. Biol. Chem.* 268: 27046–27052.

Rothschild, K. J., M. Zagaeski, and W. A. Cantore. 1981. Conformational changes of bacteriorhodopsin detected by Fourier transform infrared difference spectroscopy. *Biochem. Biophys. Res. Commun.* 103: 483–489.

Sass, H.-J., I. W. Schachowa, G. Rapp, M. H. J. Koch, D. Oesterhelt, G. Büldt, and N. Dencher. 1997. The tertiary structural changes in bacteriorhodopsin occur between M states: X-ray diffraction and Fourier transform infrared spectroscopy. *EMBO J.* 16:1484–1491.

Schneider, D. J., and J. H. Freed. 1989. Calculating slow motional magnetic resonance spectra: a users guide. *In* Biological Magnetic Resonance 8, Spin Labeling. L. J. Berliner and J. Reuben, editors. Plenum Press, New York. 1–76.

Schulten, K., and P. Tavan. 1978. A mechanism for the light-driven proton pump of *Halobacterium halobium*. *Nature.* 272:85–86.

Souvignier, G., and K. Gerwert. 1992. Proton uptake mechanism of bacteriorhodopsin as determined by time-resolved stroboscopic-FTIR spectroscopy. *Biophys. J.* 63:1393–1405.

Steinhoff, H.-J., and W. L. Hubbell. 1996. Calculation of electron paramagnetic resonance spectra from Brownian dynamics trajectories: application to nitroxide side chains in proteins. *Biophys. J.* 71:2201–2212.

Steinhoff, H.-J., K. Lieutenant, and J. Schlitter. 1989. Residual motion of hemoglobin-bound spin labels as a probe for protein dynamics. *Z. Naturforsch.* 44c:280–288.

Steinhoff, H.-J., R. Mollaaghababa, C. Altenbach, K. Hideg, M. Krebs, H. G. Khorana, and W. L. Hubbell. 1994. Time-resolved detection of structural changes during the photocycle of spin-labeled bacteriorhodopsin. *Science.* 266:105–107.

Subramanian, S., M. Gerstein, D. Oesterhelt, and R. Henderson. 1993. Electron diffraction analysis of structural changes in the photocycle of bacteriorhodopsin. *EMBO J.* 12:1–8.

Tittor, J. 1991. A new view of an old pump: bacteriorhodopsin. *Curr. Biol.* 1:534–538.

Todd, A. P., and G. L. Millhauser. 1991. ESR spectra reflect local and global mobility in a short spin-labeled peptide throughout the α-helix-coil transition. *Biochemistry.* 30:5515–5523.

Varo, G., and J. K. Lanyi. 1991. Thermodynamics and energy coupling in the bacteriorhodospin photocycle. *Biochemistry.* 30:5016–5022.

Varo, G., and J. Lanyi. 1995. Effects of hydrostatic pressure on the kinetics reveal a volume increase during the bacteriorhodopsin photocycle. *Biochemistry.* 34:12161–12169.

Wagner, G., D. Oesterhelt, G. Krippahl, and J. K. Lanyi. 1981. Bioenergetic role of halorhodopsin in halobacterium halobium cells. *FEBS Lett.* 131:341–345.

Zimany, L., Y. Cao, R. Needleman, M. Ottoleghi, and J. K. Lanyi. 1993. Pathway of proton uptake in the bacteriorhodopsin photocycle. *Biochemistry.* 32:7669–7678.